Soft Matter

Accepted Manuscript

This article can be cited before page numbers have been issued, to do this please use: A. D. Chen, M. Gandikota and A. Cacciuto, *Soft Matter*, 2026, DOI: 10.1039/D5SM01001B.

ROYAL SOCIETY OF CHEMISTRY

rsc.li/soft-matter-journal

View Article Online
DOI: 10.1039/D5SM01001B

Soft Matter

ARTICLE TYPE

Cite this: DOI: 00.0000/xxxxxxxxxx

The shape of ribbons: From polymers to surfaces

A. D. Chen[1], M. C. Gandikota[1,2] and A. Cacciuto[1*]

Received Date
Accepted Date

DOI: 00.0000/xxxxxxxxxx

Ribbons are a subset of polymerized networks that occupy an intermediate space between polymers and surfaces. We perform extensive numerical simulations to understand how to interpolate the statistical properties of ribbons across the two limits by studying their behavior as a function of their widths and bending rigidities, taking into consideration both ideal and self-avoiding ribbons. We map out a two-dimensional phase diagram of the morphology of ideal ribbons, and uncover the onset of a crumpling transition for ribbons of sufficiently large width. We also discuss the onset width above which a ribbon behaves effectively as a surface. Finally, we suggest scaling laws and functional forms that properly link and interpolate the shape of self-avoiding polymers to that of self-avoiding surfaces.

1 Introduction

Particles and molecules can be covalently linked into a wide variety of flexible structures, from simple one-dimensional (1D) linear polymers to fully two-dimensional (2D) sheets. The characterization of the morphology of these structures, which result from the interplay of entropic and enthalpic forces, is textbook material[1,2]. Given the large variety of shapes these systems can explore under the effect of thermal fluctuations (specifically in the absence of direct bending or attractive interactions), their morphology is typically classified by means of how their radius of gyration, R_g, scales with the number, N, of constituent particles/molecules, $R_g \sim N^{\nu}$. Here, the shape (or Flory) exponent ν serves as a classifier of the universality class of these structures.

While a polymer that lacks self-avoidance always crumples with a size exponent $\nu = 1/2$ on length-scales much larger than its persistence length, $l_p = k_0/k_B T$, (k_0 is the polymer bending rigidity, T the temperature, and k_B the Boltzmann factor), ideal polymerized crystalline membranes, more commonly referred to as *phantom membranes,* present a phase transition driven by their bending rigidities, κ. For small values of κ, the system is found in a crumpled state with a radius of gyrations that scales as $R_g \sim \sqrt{\log(N)}$ ($\nu = 0$), but for moderate bending rigidities ($\kappa \sim 1 k_B T$)[3] the surface expands into an extended (flat) phase characterized by $\nu = 1$[4]. The stability of the flat phase is the result of the nonlinear coupling between in-and out-of-plane thermal fluctuations which renormalizes the surface bending rigidity[5,6].

Meticulous studies of polymers and crystalline membranes form the pillars of our understanding of polymerized networks. If we now consider an $L \times L$ surface, and recursively cut it in half along the same main axial direction, or take a polymer and begin to laterally stack (polymerize) more and more polymers of the same length L in parallel to it, thus increasing the overall width, w, we obtain a ribbon which structurally interpolates a linear polymer, $w = 1$, to a polymerized surface, $w = L$. Ribbons have also been theoretically studied as developable systems whose persistence length, in the absence of thermal fluctuations, scales with their width as $l_p \sim \kappa w (k_B T)^{-1}$ [7,8]. Recently, a sophisticated form for the persistence length of ideal ribbons that accounts for the renormalization of the elastic constants by the thermal fluctuations was put forward[9,10]. Given the stark difference between the phase behavior of ideal polymers and surfaces, in that surfaces present a sharp phase transition at small bending rigidities while polymers do not, it is interesting to understand how this behavior interpolates between the two structures by using w as the tuning parameter. How do stiffness and geometry of the interpolating ribbons in thermal equilibrium depend on w? When can a ribbon be considered effectively equivalent to a surface, and how does that number relates to its overall dimensions, L and w, with $N = L \times w$. Questions of how stiffness relates to deformations away from 2D structures present a fundamental—albeit not very well explored—problem in the theory of microscopic elasticity, with important implications in a variety of fields: from graphene nanoribbons (GNRs)[11] and graphene kirigami—whose stiffness has been leveraged to construct stretchable electrodes, springs, and hinges[12]—to functional materials design, such as actuators designed from 2D skins[13].

While a recent numerical work on this subject has focused on the role of topology by studying the phase behavior of longitu-

[1] *Department of Chemistry, Columbia University, 3000 Broadway, New York, NY 10027.*
[2] *International Centre for Theoretical Sciences, Tata Institute of Fundamental Research, Bengaluru 560089, India*
* ac2822@columbia.edu

† Electronic Supplementary Information (ESI) available: [details of any supplementary information available should be included here]. See DOI: 10.1039/cXsm00000x/

View Article Online
DOI: 10.1039/D5SM01001B

dinally cleaved membrane within a flexible frame[14], connecting the behavior between a mat of polymers to that a fully connected surface, a more closely related work focused exclusively on ideal ribbons within the context of elastic frames[10,15]. Here, we also consider the behavior of self-avoiding (SA) ribbons in the absence of explicit bending forces. These SA systems better represent real physical surfaces that are not allowed to self-intersect. This is an important case to consider because, while SA polymers behave similarly to ideal polymers, albeit with a larger size exponent $\nu_F \simeq 3/5$, extensive numerical simulations have shown that self-avoiding membranes exhibit a stable flat phase even in the absence of any explicit bending rigidity [4,5], perhaps suggesting a simpler continuous connection between SA polymers and SA surfaces regulated by w.

In this paper, we systematically study the equilibrium properties of ideal ribbons as a function of w, with and without bending rigidity, and identify the onset of a crumpling transition in ideal ribbons driven by the flattening of its transversal deformations. By analyzing the normal-normal correlation function along the main long axis of the ribbon, we also identify the onset value of w beyond which an ideal ribbon behaves essentially as a surface. We study how these onsets depend on the overall length of the ribbon. Finally, we establish a simple functional form that interpolates the behavior of the radius of gyration from a fully flexible SA polymer to a fully flexible SA surface, and discuss the associated scaling law as a function of w and L.

2 Model

Our ribbons are constructed as a two-dimensional triangular fishnet of spherical particles (diameter σ) bonded together *via* harmonic springs, in a three-dimensional embedding space. Each ribbon is constructed by placing and connecting parallel polymers, each built from L beads, next to each other. Neighboring polymers are staggered by half of a bond length to enforce an overall locally hexagonal geometry in the connectivity of the beads. Our control parameter w, corresponds to the number of such parallel polymers, and is simply related to the actual physical width, $L_\perp$, of the ribbon *via* $L_\perp = \sqrt{3}/2\, w$. We consider ribbons of $w \in [1,120]$, $L \in [25, 2\cdot 10^3]$, with overall $N = L \times w \in [32, 4.8\cdot 10^4]$.

In this triangulated network, the dynamics of the particles are determined by the Langevin equation,

$$m\frac{d\mathbf{v}_i}{dt} = \mathbf{f}_i - \gamma \mathbf{v}_i + \sqrt{2D\gamma^2}\,\boldsymbol{\xi}_i(t), \tag{1}$$

m, i, and $\mathbf{v}_i$ are the particle mass, index, and velocity, respectively. γ (set to be 1) represents the translational friction, from which the translational diffusion constant can then be defined as $D = k_{\mathrm{B}}T\gamma^{-1}$, k_{B} and T being the Boltzmann constant and the temperature of the thermal bath, respectively. Solvent effects from the thermal bath are accounted for *via* the Gaussian white noise term, $\boldsymbol{\xi}_i(t)$. Importantly, $\langle \xi \rangle = 0$ and $\langle \xi_m(t)\xi_n(t')\rangle = \delta_{mn}\delta(t-t')$. The final undefined term in Eq. 1 is given by $\mathbf{f}_i = -\partial V/\partial \mathbf{r}_i$ and accounts for the conservative forces acting on each particle. Here, V is the interaction potential being differentiated and, depending the system being studied, may include the following terms,

$$\begin{aligned} V = K \sum_{\langle ij \rangle}^{\text{neighbors}} (r_{ij} - r_{\text{eq}})^2 + \kappa \sum_{\langle lm \rangle}^{\text{neighbors}} (1 - \hat{n}_l \cdot \hat{n}_m) \\ + 4\varepsilon \sum_{ij} \left[\left(\frac{\sigma}{r_{ij}}\right)^{12} - \left(\frac{\sigma}{r_{ij}}\right)^{6} + \frac{1}{4} \right], \end{aligned} \tag{2}$$

The harmonic springs bonding the particles together, present in all systems, are enforced *via* the first term of Eq. 2. Within that term, r_{eq} is defined as the equilibrium bond distance between any pair of particles given by i and j (the actual distance of a particles pair is given by r_{ij}). For self-avoiding systems, r_{eq} has a value of $1.73\,\sigma$, while for ideal systems, it has a value of $1.60\,\sigma$. While the value of the bond length is not that important for ideal surfaces, for self-avoiding surfaces it is important to select an appropriate bond length. On the one hand one should select a bond length such that no other bead can be inserted inside a triangle formed by three connected beads. This sets $\sqrt{3}\sigma$ as a the largest admissible equilibrium bond length, on the other hand a bond length that is too short can lead to non-insignificant model-dependent effective bending rigidity[16].

The strength of the particle bonds is determined by the spring constant K, which we set to $160\,k_BT/\sigma^2$. Some of our simulations also include an explicitly defined dihedral bending energy, which is enforced *via* the second term in Eq. 2. The strength of the bending term is determined by the bending rigidity κ. Unit vectors $\hat{n}_l$ and $\hat{n}_m$ represent the normals to any pair of adjacent triangles that comprise a dihedral. In the case of SA ribbons, where volume exclusion needs to be accounted for, the last term, the repulsive Weeks-Chandler-Andersen (WCA) potential[17], is present. Here, we set $\varepsilon = k_BT$. To numerically integrate the Langevin equation, we use the numerical package LAMMPS[18]. In these simulations, we use σ, $k_{\mathrm{B}}T$, and $\tau = \sigma^2 D^{-1}$ as our unit length, energy, and time, respectively. Our simulation timestep lengths range from $\Delta t = 0.01\,\tau$ to $0.03\,\tau$.

3 Ideal Ribbons

3.1 Zero bending rigidity

We first consider the case of an ideal ribbon in the absence of bending rigidity. Our numerical results for a fixed value of L as a function of w, shown in Fig. 1, indicate that the radius of gyration of the ribbon decreases monotonically with w and the simple functional form $R_g = \alpha\,(L/w)^{1/2} + \beta\sqrt{\log w} + \gamma$ that interpolates the two limiting behaviors, does a good job at capturing the overall trend of the data points. This function, for $w \to 1$, simplifies to the ideal random-walk scaling $R_g \sim L^{1/2}$, and for $w \to L$, it reduces to the scaling of a crumpled ideal membrane $R_g \sim \sqrt{\log L}$. We notice that this functional form is a bit different than that obtained for ideal cleaved membranes in the absence of bending rigidity as discussed in our recent paper[14], and better fits the data for the ribbon at large values of w. It is also instructive to look at the size dependence of this behavior while keeping w constant. If fact, while in the strict limit of $w = 1$ we expect a simple size exponent of $\nu = 1/2$ (with L), for an intermediate value of w it is not immediately clear what controls the scaling of the ribbon. Figure 2

View Article Online
DOI: 10.1039/D5SM01001B

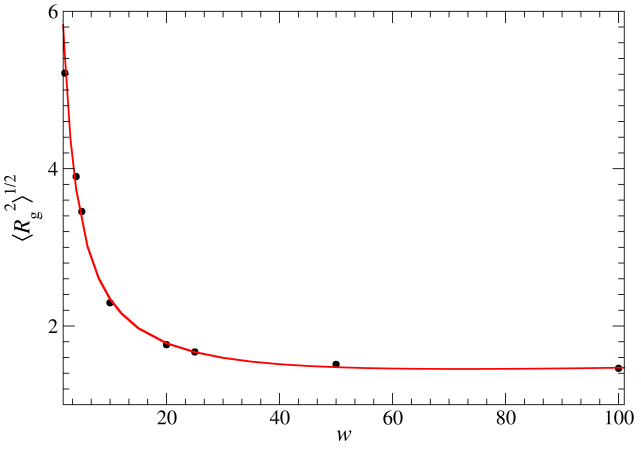

Fig. 1 Radius of gyration R_g of an ideal ribbon in the absence of bending energy as a function of its width, w, and a fixed $L = 100$. The red curve is a fit to the data using the interpolating functional form $R_g = \alpha (L/w)^{1/2} + \beta\sqrt{\log(w)} + \gamma$, where $\alpha = 1.3818$, $\beta = 3.36435$, and $\gamma = -7.13197$.

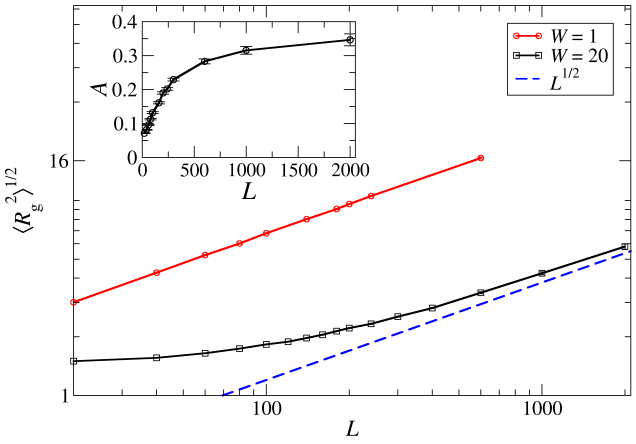

Fig. 2 Radius of gyration R_g of an ideal ribbon in the absence of bending energy as a function of its length L, for width $w = 1$ (in red) and $w = 20$ (in black). The blue dashed line indicates the reference $L^{1/2}$ power law. Inset: Asphericity A[19] of the ribbon at a fixed $w = 20$ as a function of L.

shows in a log-log plot the reference scaling of R_g with L for a ribbon of width $w = 1$ (a reference ideal polymer), and the same scaling for $w = 20$. Interestingly, for $w = 20$, the slope of the curve begins quite flat for small values of L, corresponding to the scaling behavior of a crumpled ideal surface, and eventually it recovers the polymer-like scaling in the limit of large L. Correspondingly, the inset of the same figure shows how the asphericity[19], defined as $A \equiv 3/2\,(\lambda_1^2 + \lambda_2^2 + \lambda_3^2)/(\lambda_1 + \lambda_2 + \lambda_3)^2 - 1/2$, where λ_i's are the eigenvalues of the shape tensor so that $R_g^2 = \lambda_1 + \lambda_2 + \lambda_3$, is close to zero (as expected for an isotropic crumpled ideal membrane) for small values of L, and monotonically grows to near 0.35 for large values of L ($A \approx 0.396$ for an ideal polymer in the $L \to \infty$ limit[20]). Conversely, data at a fixed aspect ratio L/w indicate that R_g is rather insensitive to the value of L (data not shown), consistent with the expected dependence obtained by our fitting function $R_g \sim \sqrt{\log w}$. Despite our best efforts we were unable to find a master curve that simultaneously accounts for the dependence on L and w.

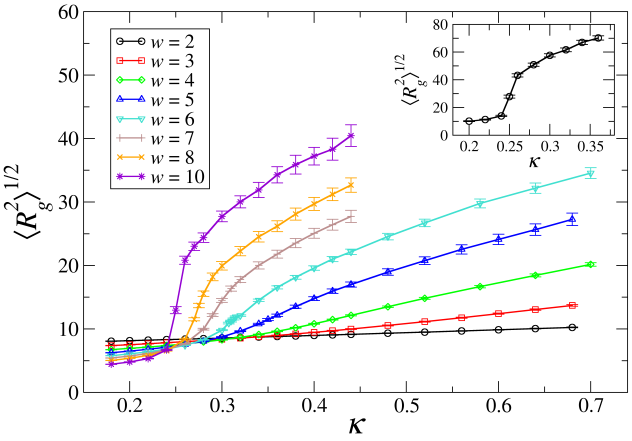

Fig. 3 Radius of gyration of a ribbon, R_g, as a function of its bending rigidity κ for ideal ribbons of different width, w, and fixed length $L = 200$. The inset shows the same plot for an ideal ribbon of length $L = 1000$ and width $w = 10$.

3.2 Finite bending rigidity

We now consider the case where an explicit bending rigidity, κ, is added to the system. We know that a bending rigidity causes a crumpled to flat transition in ideal tethered surfaces at a critical κ^* that is quite small (under $1\,k_BT$). Below (above) κ^* the membrane exists in a crumpled (flat) phase with $R_g \sim \log L$ ($R_g \sim L$), respectively[4]. To characterize the size of ribbons with different widths by equal longitudinal length, L, here we use the radius of gyration R_g of the central spine of the ribbon. This allows us a consistent basis for comparing ribbons of different widths w.

3.2.1 Onset of the crumpling transition

Fig. 3 shows how R_g depends on the bending rigidity κ for different values of the width of the ribbon. For small values of w, we can see in Fig. 3, a smooth monotonic increase in R_g as κ is increased, corresponding to a gradual expansion/extension of the ribbon as it becomes more rigid, consistent with the behavior of ideal rigid polymers. However, deviations from a simple linear behavior expected in the strict polymer limit, are already visible for $w = 3$, where an upward bend of the curve is clearly visible and becomes more apparent for smaller values of κ as we increase w. For larger values of w, the upward bend in the curves transforms into a discontinuity in R_g with κ, suggesting a transition where the ribbon expands from a very compact object to a more extended one. The steepness of the jump increases systematically with w, and indicates the presence of a crumpling transition even for very thin ribbons.

To establish and identify the onset of this transition with w, we calculate the specific heat[21] by measuring $c_{\text{bend}} = \langle E_{\text{bend}}^2 \rangle - \langle E_{\text{bend}} \rangle^2$ where E_{bend} is the bending energy per particle; variations in stretching energy are negligible. For a given width w, we calculated $c_{\text{bend}}(\kappa)$ for different system sizes L (Fig. 4). For $w = 2$ (Fig. 4a), c_{bend} smoothly and monotonically increases. For intermediate widths w ($w = 7$ and $w = 8$; Fig. 4b, c), we observe a peak in $c_{\text{bend}}(\kappa)$. The height of the peak in these curves has a weak but clear size dependence on L (Fig. 4c), indicative of the onset of a continuous phase transition, which is fully exposed for $w = 10$

View Article Online
DOI: 10.1039/D5SM01001B

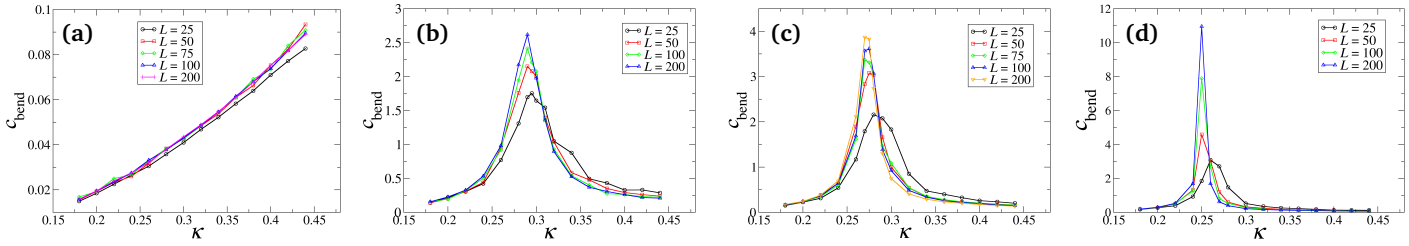

Fig. 4 The specific heat of ideal ribbons c_{bend} as a function of the bending rigidity κ for different lengths, L with widths (a) $w = 2$, (b) $w = 7$, (c) $w = 8$, and (d) $w = 10$.

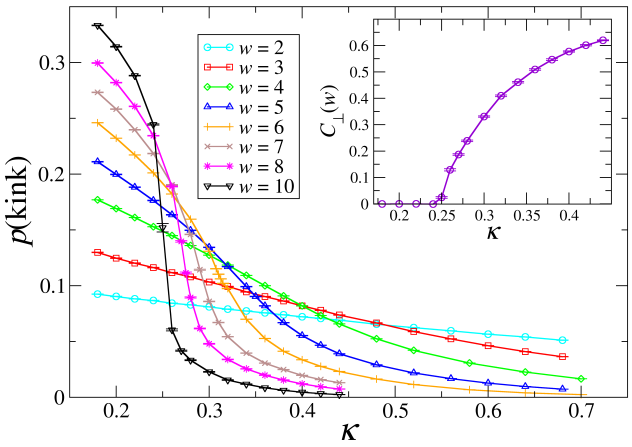

Fig. 5 Probability of finding a kink $p(\mathrm{kink})$ along the backbone of an ideal ribbon as a function of its bending rigidity κ, for different values of the width w. The inset shows the transversal correlation function $C_\perp(w)$ between the first polymer forming the ribbon and the last (at a distance $w = 10$), as a function of κ. All data are for a ribbon of length $L = 200$.

(Fig. 4d). We set $w^* \approx 10$ as the onset width above which a phase transition begins to occur as the rigidity of an ideal ribbon is increased, because the specific heat for smaller values of w tends to saturate with L while for $w = 10$ we observe a more distinct and systematic increase. Furthermore, $w = 10$ is also accompanied by a significant discontinuity in the R_g versus κ plot, that is not as evident for smaller values of w.

These results suggest that beyond w^*, an ideal ribbon acquires one of the main characteristic features of a surface: a crumpling transition. Crucially, the onset w^* value is rather independent of L. As shown in the inset of Fig. 3, where we computed R_g as a function of κ for a ribbon of length $L = 1000$ and $w = 10$, and the same jump in R_g is present at around the same value of $\kappa \simeq 0.25$. This result is quite important because it defines a clear departure from our previous data on ideal ribbons in the absence of bending rigidity for which the polymer limit was recovered upon increasing the L/w ratio. Clearly, this is no longer the case as soon as bending energy is introduced in the system.

3.2.2 Kinks in the ribbon

To further characterize the state of the ribbon, we also employ another order parameter—the proportion of kinks[22] $p(\mathrm{kink})$ along the spine of the ribbons. The angle between the oriented normals of any two adjacent triangles along the ribbon mid-line is counted as a kink if this angle exceeds a threshold angle of 160 degrees (the angle is zero degrees when triangles are flat), and $p(\mathrm{kink}) = n_{\mathrm{kink}}/L$. The results are shown in Fig. 5, which plots $p(\mathrm{kink})$ for several values of w for constant $L = 200$. We can see that for small w, the $p(\mathrm{kink})$ shows a gradual decline towards 0 as κ is increased, corresponding to the gradual unfolding of the kinks as the ribbon becomes smoother. At $w = 10$, as κ is increased, we see a sharp drop in $p(\mathrm{kink})$ as we cross $\kappa^* \approx 0.25$, signaling the presence of the crumpling transition.

A key difference between the transition observed in ribbons and that observed in surfaces, is that the transition in the latter case drives the surface from a crumpled phase directly into a flat extended state. This is not the case for ribbons. For small values of w, the shape of the ribbons beyond the transition is not a flat/extended conformation, but rather a smooth curled state, with sporadic sharp folds (kinks). This is quite evident from images of the simulation data, but also from the normal-normal correlation function along the backbone of the ribbon, which decays to zero at lengths smaller than L (data not shown).

Crucially, what seems to be tracking the transition is the lateral (transversal) correlation length. In the inset of Fig. 5, we plot $C_\perp(w) = \langle \hat{n}_1 \cdot \hat{n}_w \rangle$, where $\hat{n}_1$ and $\hat{n}_w$ correspond to the normals of the first and last triangles across the ribbon width, respectively, averaged along the ribbon backbone as a function of κ for $w = 10$. This result suggests that, for sufficiently wide ribbons, the transition occurs when $l_p \geq w$, i.e. when the ribbons become transversally flat.

3.2.3 Structural phase diagram

Recently, Košmrlj et al.[9,23] provided an expression for the persistence length of a ribbon that accounts for the renormalization of the bending rigidity in the presence of thermal fluctuations:

$$l_{\mathrm{p}} = \frac{2\kappa_{\mathrm{R}} w}{k_{\mathrm{B}} T} \tag{3}$$

where $\kappa_{\mathrm{R}} = \kappa(w/\ell_{\mathrm{th}})^{\eta}$ is the renormalized bending rigidity, $\ell_{\mathrm{th}} = \sqrt{64\pi^3 \kappa^2/(3k_{\mathrm{B}}TY)}$ is the thermal length of the ribbon, the exponent $\eta = 0.8$ and $Y = 2K/\sqrt{3}$ is the surface Young modulus (K is the bond strength). Using Eq. 3 and imposing the condition $l_p = w$ we obtain $\kappa^* \sim w^{-\eta/(1-\eta)} \sim w^{-4}$. Clearly, this simple expression cannot determine the onset transition point of the system, but suggests that the transition point κ^* should decrease

View Article Online
DOI: 10.1039/D5SM01001B

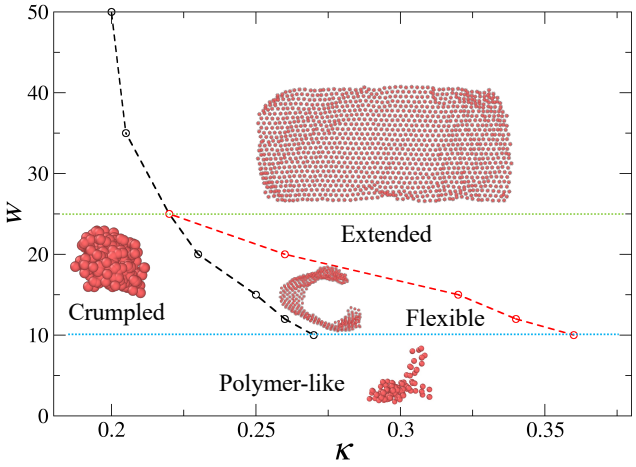

Fig. 6 Structural phase diagram of an ideal ribbon in terms of its bending rigidity κ and its width w. The images are snapshot of our model from simulations depicting the typical configurations of the ribbon. This diagram has been constructed using a ribbon of length $L = 50$.

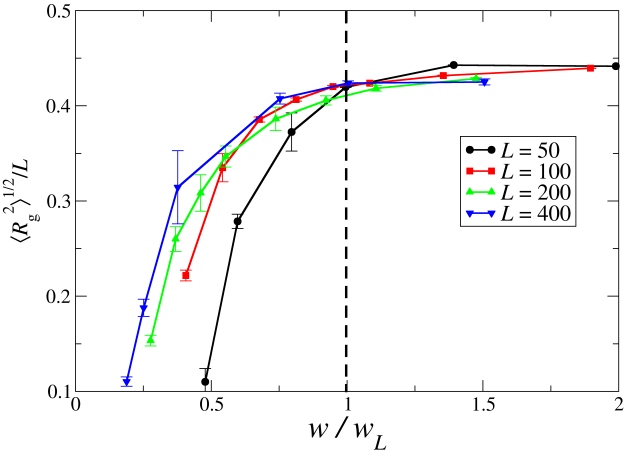

Fig. 7 Radius of gyration of the ribbon's backbone normalized by its length L as a function of the relative width w/w_L, for different values of L. Here $w_L = (L/A_0)^{1/(1+\eta)}$, with $A_0 = 0.15$ and $\eta = 0.8$. The black vertical dashed line highlights the point where $w/w_L = 1$.

with the width of the ribbons w, and this is indeed what we observe. A systematic study of the behavior of a ribbons of a fixed length $L = 50$ for different widths allows us to generate a structural phase diagram connecting the behavior of polymers, ribbons and surfaces. The results are summarized in Fig. 6. The blue dotted line indicates the boundary below which the ribbon continuously increases in size with κ bypassing the crumpling transition. The black dashed line delineates the boundary between the crumpled and the extended phase. This rough boundary was obtained by running a number of simulations starting from a flat configuration and finding the value of κ for which a ribbon undergoes a sudden drop in R_g. Finally, the red dashed line serves to distinguish between transversally flat but smooth and flexible ribbons and longitudinally straight/rigid/flat ones. Because it can sometimes be quite difficult to visually distinguish between the flexible and flat ribbons, especially in cases of smaller w, given the continuous nature of this crossover, we obtain this boundary by computing the full longitudinal normal-normal correlation function along the mid long axis of the ribbon $C_{\parallel}(s) = \langle \hat{n}(r) \cdot \hat{n}(r+s) \rangle$, and asking that this function does not decay to zero for $s < L$.

We define the intersection between the dashed black and the dashed-red line as the value of w above which a ribbon goes directly from a crumpled to a flat state, and we take this point, $w \simeq 25$, as the onset value above which a ribbon is basically indistinguishable from a surface. The green dotted line establishes this boundary. This onset value is also consistent with the behavior of R_g versus κ for $w = 25$: beyond the critical point, R_g jumps directly to a large value that is largely insensitive to further increases in κ. In contrast, for smaller w, R_g increases gradually toward the same value.

We expect the value of this upper onset, w_L, to be dependent on the length of the ribbon L. Indeed, the flattening of the ribbon should occur when $l_p \geq L$. Using the definition of l_p given in Eq. 3, and assuming a fairly constant critical bending rigidity $\kappa^* \simeq 0.22$, we have that $l_p \simeq A_0 w^{1+\eta}$, where $A_0 \simeq 0.15$ is a model dependent prefactor that we fix by imposing that $l_p(w = 25) = 50$. We would therefore expect $w_L \simeq (L/A_0)^{1/(1+\eta)} = (L/A_0)^{0.55\bar{5}}$. This expectation is consistent with our numerical simulations for $L = 100$, $L = 200$, and $L = 400$, where we indeed find that just above the critical rigidity at $\kappa = 0.24$, the radius of gyration dependence on w becomes essentially constant when $w > w_L$. Figure 7 reports on how the radius of gyration of the backbone of the ribbon normalized by its length depends on the ratio w/w_L, and indicates that for $w/w_L > 1$, the ribbon is essentially flat.

These results set two important boundaries $w^* \simeq 10$ and $w_L \simeq (L/A_0)^{0.55\bar{5}}$ in the phase behavior of ideal ribbons as one interpolates between polymers and surfaces, and provide firmer ground for some of the results suggested in [15,24], where this crumpling transition was first observed in the context of elastic frames – ribbons of different widths here are generated by radially removing material from the core of a membrane, and $w^* = 12$ was suggested as the onset value for the transition.

4 Self-Avoiding Ribbons

We now consider self-avoiding ribbons in the absence of any explicit bending rigidity. We already know that a SA surface remains flat and a SA polymer scales with a Flory exponent of 3/5. It is therefore reasonable to assume that the width of the ribbon should act as a source of rigidity as it is the case for ideal ribbons with constant bending energy (in that case $l_p \sim \beta \kappa w$).

It is tempting to map the behavior of the radius of gyration of a SA ribbon of increasing width to that of a SA polymer with increasing bending energy, k_0 (persistence length). We find that while for a polymer these curves, R_g vs k_0, for different polymer lengths can be collapsed into a single master curve when normalized by L [25] (see inset of Fig. 8), the same collapse, now in terms of R_g vs w, does not hold for ribbons (Fig. 8). Instead, we find that the unrescaled dependence between R_g and w can be well described by a simple hyperbolic tangent of the form $f(w) = \alpha \tanh(\beta w) + \gamma$ (see inset of Fig. 9). Furthermore, all the data can be made to collapse (apart for some finite size effects) when, rather than the bare width of the ribbon, we plot

View Article Online
DOI: 10.1039/D5SM01001B

(see Fig. 9) the radius of gyration in terms of the ratio between its persistence length $l_p \sim w^{1.8}$ as obtained for the ideal ribbons with a given bending energy as discussed in Eq. 3, and the ribbon's length, L. Assuming $l_p = b_0 w^{1.8}$, we estimated the prefactor b_0 by extracting l_p from a fitting of the normal-normal correlation function of the ribbons for three different widths $w = 4, 6$ and 12, for which a clear exponential decay is observed. We then imposed the measured l_p to be equal to $b_0 w^{1.8}$ for each of those given w, and obtained consistently a value of $b_0 \simeq 0.19$. The collapsed data can likewise be fit with the functional form $f(x) = \alpha \tanh(\beta x^{\delta}) + \gamma$, where $x = l_p/L$ (see Fig. 9), and $\delta \approx (1/1.8)$, thus implying a linear dependence of R_g with w for thin ribbons.

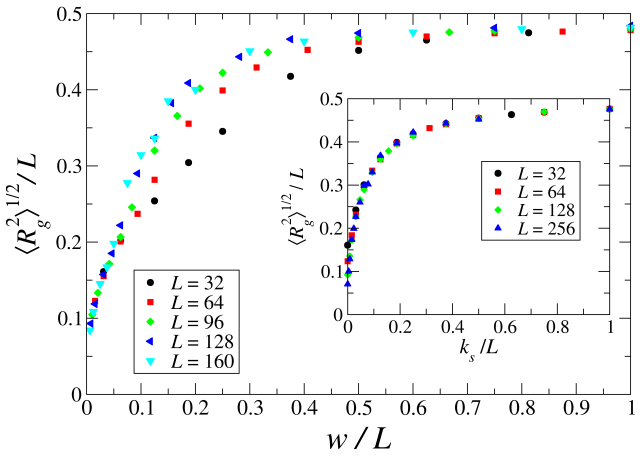

Fig. 8 Collapse failure of the radius of gyration, R_g (normalized by L), of the backbone of a SA ribbon as a function of w/L for ribbons of different length. (Inset) Excellent collapse of the radius of gyration, R_g (normalized by L), as a function of its bending rigidity k_0 (also normalized by L) for a polymer of different lengths.

It should be pointed out that although an explicit bending energy term is not present in our system and self-avoidance, that is a non-local interaction, cannot be in general mapped into an explicit bending rigidity, as discussed in the methods section, it is known that a very small effective local rigidity can arise from the surfaces' discretization and the non-intersection of self-avoiding beads at the nodes of the surface. This is because the normals to two adjacent triangles can be parallel but not fully antiparallel in a bead and spring model[16] and this can lead to an effective rigidity of the order of $1 k_B T$. It is therefore not unreasonable that the persistence length of a rigid ideal ribbon also holds for SA ribbons; after all in the limit for $w \to L$, SA surfaces and rigid ideal membranes belong to the same universality[5,26], and this has been tested using bead-free models where self-avoidance was forbidden by explicitly checking triangle-triangle intersections[26,27].

Overall, our numerical data suggest that for SA ribbons, it is possible to interpolate the radius of gyration of a polymer to that of a tethered surface, and, beyond the Sadowsky[8] approximation, using the appropriate renormalized persistence length, one can rescale the all data into a single master curve for any ribbon's length L and width w.

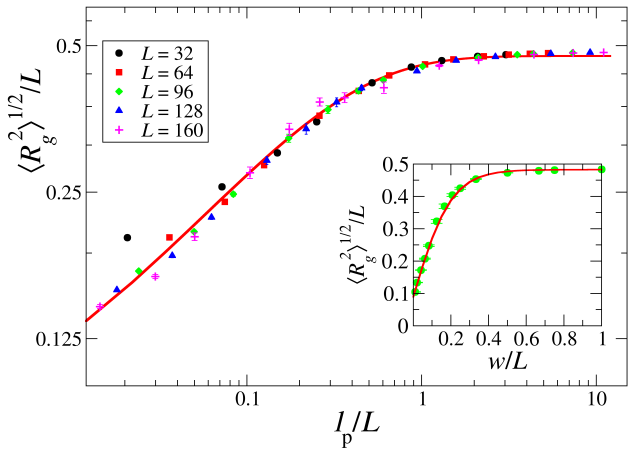

Fig. 9 Collapse in log-log scale of the radius of gyration, R_g (normalized by L), of the backbone of a SA ribbon as a function of its renormalized persistence length l_p, rescaled by L for ribbons of different length. The solid line is a fit to the data with the function $f(x) = \alpha \tanh(\beta x^{\delta}) + \gamma$, with $\alpha = 0.41(2)$, $\beta = 1.8(1)$, $\gamma = 0.06(1)$ and $\delta = 0.52(5)$. (Inset) Radius of gyration, R_g as a function of the ribbon width, w (both normalized by L) for $L = 96$. The solid line is a fit to the data using the function $f(w) = \alpha \tanh(\beta w) + \gamma$, with $\alpha = 0.394(3)$, $\beta = 4.9(2)$, and $\gamma = 0.088(3)$.

5 Conclusions

Although a significant amount of work has been done to understand polymers, ribbons and surfaces, independently of each other, to the best of our knowledge this is the first attempt to systematically study the behavior of these three fundamental building blocks of matter with the aim of interpolating their phase behavior within the same framework. The only previous work in this direction[15,24], focused exclusively on ideal systems in the context of elastic frames. Here, we extended that work by performing more systematic numerical simulations. We present a full phase diagram identifying the morphology of ideal ribbons as a function of both their bending rigidity and width. We also explore explicitly the case of SA ribbons. For ideal ribbons, we find a clear bound setting the onset of a crumpling transition $w^* \simeq 10$, and discuss how this number is universal and independent of ribbon length. We also discuss the onset value of the width above which a ribbon behaves essentially as a surface and suggest its dependence on the ribbon's length to be $w_L \simeq (L/A_0)^{0.55}$, where A_0 is a model dependent prefactor. We explore the finite size scaling of ideal ribbons in the absence of bending rigidity.

Finally, we explore the behavior of SA ribbons where we interpolate their statistical properties from SA polymers to SA surfaces. Here, we find that the interpolating ribbon can be thought of as a polymer whose persistence length is not proportional to the bare width of the ribbon as expected for vary thin ribbons in the Sadowsky limit (see [8,28,29] and references therein), but with the persistence length proposed in[9,23], which accounts for the renormalization of the elastic constants due to thermal fluctuations. Furthermore, we also find that for a fixed length the radius of gyration of a ribbon as a function of its width is very well described by a simple hyperbolic tangent functional form, which recovers the Sadowsky limit[8] for small values of w. It is

View Article Online
DOI: 10.1039/D5SM01001B

worth pointing out that the functional dependence of R_g for ideal and self-avoiding ribbons is quite different than that observed for a system of cleaved membranes[14], as a function of the spacing between the cuts (width of the ribbons). While the cleaved membrane system also connect the behavior of polymers (a number of them, connected within a flexible polymer frame, for large number of cuts) and that of a surface (no cuts), here, we observe a much sharped dependence of R_g on w for single unconstrained ribbons. This difference is even starker for self-avoiding surfaces that for cleaved membranes has a non-monotonic behavior with the width of the slices. Although a one-to-one comparison between the two systems is not straightforward as the two systems have different degrees of freedom, for instance, apart from the frame connecting the polymers for small w, the number of particles in the cleaved membrane system also remains constant, it would be nevertheless interesting to see whether ideal cleaved membranes also exhibit a transition as a function of the bending rigidity below some threshold value of the number of cuts.

We hope that our result will stimulate more work in this direction.

Data availability

Data for this article, including all data points in the figures and the codes used to run the trajectories are available at the repository that can be found on the Cacciuto Group website at `https://www.columbia.edu/cu/chemistry/groups/cacciuto/research.html`.

Conflicts of interest

There are no conflicts to declare.

Acknowledgements

A.C. acknowledges financial support from the National Science Foundation under Grant No. DMR-2321925.

References

1 M. Rubinstein and R. H. Colby, *Polymer physics*, Oxford university press, 2003.
2 P. M. Chaikin, T. C. Lubensky and T. A. Witten, *Principles of condensed matter physics*, Cambridge university press Cambridge, 1995, vol. 10.
3 Y. Kantor, M. Kardar and D. R. Nelson, *Physical review letters*, 1986, **57**, 791.
4 D. Nelson, S. Weinberg and T. Piran, *Statistical Mechanics of Membranes and Surfaces (Second Edition)*, World Scientific Publishing Company, Singapore, 2004.
5 M. J. Bowick and A. Travesset, *Phys. Rep.*, 2001, **344**, 255–308.
6 K. J. Wiese, in *Phase transitions and critical phenomena Vol 19*, ed. C. Domb and J. L. Lebowitz, Elsevier, 2001, pp. 253–480.
7 L. Giomi and L. Mahadevan, *Phys. Rev. Lett.*, 2010.
8 M. Sadowsky, *Preuss. Akad. Wiss*, 1930, 412–415.
9 A. Košmrlj and D. R. Nelson, *Physical Review B*, 2016, **93**, 125431.
10 D. Yllanes, S. S. Bhabesh, D. R. Nelson and M. J. Bowick, *Nature communications*, 2017, **8**, 1381.
11 H. Wang, H. S. Wang, C. Ma, L. Chen, C. Jiang, C. Chen, X. Xie, A.-P. Li and X. Wang, *Nat. Rev. Phys.*, 2021, **3**, 791–802.
12 M. K. Blees, A. W. Barnard, P. A. Rose, S. P. Roberts, K. L. McGill, P. Y. Huang, A. R. Ruyack, J. W. Kevek, B. Kobrin, D. A. Muller and P. L. McEuen, *Nature*, 2015, **524**, 204–207.
13 A. Rafsanjani, Y. Zhang, B. Liu, S. M. Rubinstein and K. Bertoldi, *Sci. Robot.*, 2018, **3**, eaar7555.
14 A. D. Chen, M. C. Gandikota and A. Cacciuto, *Soft Matter*, 2025, **21**, 1134–1140.
15 D. Yllanes, D. R. Nelson and M. J. Bowick, *Phys. Rev. E*, 2019, **100**, 042112.
16 F. F. Abraham and D. R. Nelson, *J. Phys.*, 1990, **51**, 2653–2672.
17 J. D. Weeks, D. Chandler and H. C. Andersen, *J. Chem. Phys.*, 1971, **54**, 5237–5247.
18 S. Plimpton, *J. Comput. Phys.*, 1995, **117**, 1–19.
19 J. Rudnick and G. Gaspari, *J. Phys. A*, 1986, **19**, L191.
20 M. Bishop and C. J. Saltiel, *J. Chem. Phys.*, 1988, **88**, 3976–3980.
21 Y. Kantor and D. R. Nelson, *Phys. Rev. A Gen. Phys.*, 1987, **36**, 4020–4032.
22 R. Golestanian and T. B. Liverpool, *Physical Review E*, 2000, **62**, 5488.
23 P. Z. Hanakata, S. S. Bhabesh, M. J. Bowick, D. R. Nelson and D. Yllanes, *Extreme Mech. Lett.*, 2021, **44**, 101270.
24 D. Yllanes, S. S. Bhabesh, D. R. Nelson and M. J. Bowick, *Nat. Commun.*, 2017, **8**, 1–8.
25 R. A. Pethrick, *Br. Polym. J.*, 1988, **20**, 299.
26 M. J. Bowick, A. Cacciuto, G. Thorleifsson and A. Travesset, *The European Physical Journal E*, 2001, **5**, 149–160.
27 D. M. Kroll and G. Gompper, *J. Phys. I*, 1993, **3**, 1131–1140.
28 L. Giomi and L. Mahadevan, *Phys. Rev. Lett.*, 2010, **104**, 238104.
29 E. H. Yong, F. Dary, L. Giomi and L. Mahadevan, *Proc. Natl. Acad. Sci. U.S.A.*, 2022, **119**, e2122907119.

View Article Online
DOI: 10.1039/D5SM01001B

Data for this article, including all data points in the figures and the codes used to run the trajectories are available at the repository that can be found on the Cacciuto Group website at https://www.columbia.edu/cu/chemistry/groups/cacciuto/research.html.